Two-Photon–NIR-II Antimicrobial Graphene-Nanoagent for Ultraviolet–NIR Imaging and Photoinactivation

WEN-SHUO KUO (wenshuokuo@mail.ncku.edu.tw)
National Cheng Kung University
Chia-Yuan Chang
National Cheng Kung University
Ping-Ching Wu
National Cheng Kung University
Jiu-Yao Wang
National Cheng Kung University

Research

Keywords: Sorted-graphene quantum dot, Excitation-wavelength-independent photoluminescence, 960-nm-two-photon-excitation-wavelength, Two-photon photoinactivation, Near-infrared-II two-photon imaging

Posted Date: May 18th, 2021

DOI: https://doi.org/10.21203/rs.3.rs-519688/v1

Abstract

Background

Nitrogen doping and amino-group functionalization, which result in strong electron donation, can be achieved through chemical modification. Large π-conjugated systems of graphene quantum dot (GQD)-based materials acting as electron donors can be chemically manipulated with low two-photon excitation energy in a short photoexcitation time for improving the charge transfer efficiency of sorted nitrogen-doped amino acid–functionalized GQDs (sorted amino-N-GQDs).

Results

In this study, a self-developed femtosecond Ti-sapphire laser optical system (222.7 nJ pixel^{-1} with 100-170 scans, approximately 0.65-1.11 s of total effective exposure times; excitation wavelength: 960 nm in the near-infrared II region) was used for chemical modification. The sorted amino-N-GQDs exhibited enhanced two-photon absorption, post-two-photon excitation stability, two-photon excitation cross-section, and two-photon luminescence through the radiative pathway. The lifetime and quantum yield of the sorted amino-N-GQDs decreased and increased, respectively. Furthermore, the sorted amino-N-GQDs exhibited excitation-wavelength-independent photoluminescence in the near-infrared region and generated reactive oxygen species after two-photon excitation. An increase in the size of the sorted amino-N-GQDs boosted photochemical and electrochemical efficacy and resulted in high photoluminescence quantum yield and highly efficient two-photon photodynamic therapy.

Conclusion

The sorted dots can be used in two-photon contrast probes for tracking and localizing analytes during two-photon imaging in a biological environment and for conducting two-photon photodynamic therapy for eliminating infectious microbes.

Background

Graphene quantum dot (GQD)-based materials with $\pi-\pi$ configuration and surface groups exhibit a high surface area, large diameter, and excellent surface grafting. These materials may contribute to intrinsic-state and defect-state emissions to achieve photoluminescence (PL). Intrinsic-state emissions are induced by the quantum size effect, zigzag edge sites, or recombination of localized electron–hole pairs, whereas defect-state emission originates from the defect effect (energy traps) [1, 2]. The PL emission of a material determines its suitability for imaging and photochemistry [3]. GQDs can be bonded with nitrogen atoms (N-GQDs) to alter their chemical composition and modulate their band gap, thereby enhancing photochemical properties and facilitating tunable luminescence in bioimaging and photodynamic (or photoinactivation) applications [4, 5]. Furthermore, primary amine molecules (also known as amino-group functionalization) can be chemically modified to realize strong electron donation for considerably altering

the electronic properties of nitrogen-doped amino acid–functionalized GQD (amino-N-GQDs) materials, thereby augmenting electrochemical and photochemical activities [6].

An effective approach can be realized for investigating photoexcitation by combining multiphoton and near-infrared (NIR) excitations. This approach has a lower absorption and shorter photoexcitation period than other types of excitations. Furthermore, this approach exhibits ultralow energy consumption. Because of these attributes, deep penetration of biological specimens and effective observation are possible. This study used a novel femtosecond Ti-sapphire laser optically inverted microscopy system (a repetition rate of 80 MHz; Mai Tai with the optical parametric oscillators; Spectra-Physics, USA; Scheme 1). Moreover, given the possible excitation–wavelength–dependent PL phenomenon caused by the derived amino-N-GQDs featuring quantum confinement in the sp^2 domains and intrinsic-state and defect-state emissions, this study revealed that sorted amino-N-GQDs sieved by membranes with the pores of various sizes bearing homogeneous atom dopant functionalities enabled investigation of the electronic and intrinsic properties related to the optical behavior with the quantum-confinement effect [7]. This phenomenon resulted in excitation–wavelength–independent two-photon luminescence (EWI-TPL) emission under the two-photon excitation (TPE) wavelength extending to 960 nm in the NIR-II region [8, 9]. X-ray photoelectron spectroscopy (XPS) revealed that with the enlargement of sorted amino-N-GQDs, the numbers of the C-N group, pyridinic-, amino-, and pyrrolic-N functionalities increased. This increase can induce a radiative recombination of localized electron–hole pairs, resulting in conspicuous two-photon properties, including favorable two-photon absorption (TPA), high TPL emission, excellent absolute TPE cross-sections, short lifetime, high ratio of radiative-to-nonradiative decay rates, and high post-TPE stability. Moreover, an increase in the mean lateral size results in a high PL quantum yield (QY) and highly efficient photodynamic therapy (PDT, or photoinactivation) action under TPE (Ex: 960 nm, an ultralow energy of 222.7 nJ $pixel^{-1}$ with the short photoexcitation period of 100–170 scans, total effective exposure times of approximately 0.65–1.11 s). The current results indicated that sorted amino-N-GQDs can function as a promising two-photon contrast probe in tracking and localizing analytes with in-depth two-photon imaging of a biological environment on two-photon-PDT to eliminate infectious microbes easily.

Materials

Preparation of amino-N-GQDs and sorted amino-N-GQDs

Amino-N-GQDs: graphene oxide was prepared from a natural graphite powder (Bay carbon Inc., USA) using a modified Hummers' method [10]. Graphite (8.5 M) and $NaNO_3$ (0.6 M) (Merck & Co., USA) were mixed with H_2SO_4 (18M; Sigma Aldrich Co., St Louis, USA). $KMnO_4$ (2.0 M; FUJIFILM Wako Chemicals USA Inc., USA) was slowly added with continual stirring at 35°C overnight. Subsequently, ddH_2O was gradually added and continually stirred. H_2O_2 (35 %; Sigma Aldrich Co., USA) was added to terminate the reaction. Washing and centrifugation with ddH_2O were performed several times, and the graphene oxide was collected. The as-prepared graphene oxide was placed in a tube furnace and heated to 400–600°C in

the presence of $NH_{3(g)}$ for 4–6 h; it was subsequently introduced to concentrated HNO_3 (16.0 M; Sigma Aldrich Co., USA) and stirred for 2 days. The mixture was placed in a sonicator for 2 days and subsequently placed in an oven at 160°C for 1 day to vaporize all the liquid. Washing and centrifugation (83000 rpm; Optima TLX Ultracentrifuge, Optima TLX Ultracentrifuge, Beckman Coulter Inc., USA) with ddH_2O were conducted several times. The supernatant was filtered through a 0.22 μm microporous membrane. The pH of the resulting black suspension was tuned to 7.4 with NaOH (1M; Sigma Aldrich Co., USA), and it was stayed in a dialysis bag (retained molecular weight: 300 kDa) > 12 h, and N-GQDs were obtained. The as-prepared N-GQDs were mixed with $NH_{3(aq)}$ (28 %; Sigma Aldrich Co., USA), stored in a Teflon-lined stainless steel autoclave, and reacted at 180°C for 5 h. The resulting mixture was washed with ddH_2O, centrifuged several times, and subsequently dried in an oven at 50°C overnight. Eventually, amino-N-GQDs were obtained (Additional file, Scheme S1a).

Sorted-amino-N-GQDs: the amino-N-GODs were sieved using centrifugation tubes equipped with polypropylene membranes filters with cut-off molecular weights of 300, 100, and 50 kD (Satorius, Germany). The amino-N-GOD suspension was flowed through membranes arranged in a sequence of decreasing pore size and collected at serial stages to form the sorted amino-N-GQDs of varying sizes, yielding mean lateral sizes of 9.1 ± 0.2 nm (amino-N-GQD 9.1), 9.9 ± 0.2 nm (amino-N-GQD 9.9), 11.1 ± 0.3 nm (amino-N-GQD 11.1), and 12.0 ± 0.4 nm (amino-N-GQD 12.0).

All Materials section for this article can be found in the Additional file.

Results And Discussion

Characterization of material and investigation of two-photon property

Amino-N-GQDs were synthesized from graphene oxide sheets through ultrasonic shearing according to the modified Hummers method [10] (Additional file, Fig. S1, Table S1 and Scheme S1a). The as-prepared amino-N-GQDs with homogeneous oxygen (O) and N distributors exhibiting high crystallinity and uniformity were sieved by membranes with pores of various sizes. Low-magnification (Additional file, Figs. S2a–d) high-resolution transmission electron microscopy (HR-TEM; Additional file, Figs. S2e-h) was used to characterize the amino-N-GQDs. The mean lateral sizes of the sorted dots were set at 9.1 ± 0.2 nm (amino-N-GQD 9.1), 9.9 ± 0.2 nm (amino-N-GQD 9.9), 11.1 ± 0.3 nm (amino-N-GQD 11.1), and 12.0 ± 0.3 nm (amino-N-GQD 12.0). Other characterizations helped successful preparation of sorted amino-N-GQDs (Additional file, Figs. S3–S5).

Recombination of zigzag edge sites, localized electron–hole pairs, and quantum effect are used to induce intrinsic-state emission of GQD-based materials, whereas the defect effect (energy traps) triggers defect-state emission [2, 5, 6]. To demonstrate the effect, Fig. 1a displays sorted amino-N-GQDs dispersions, various levels of PL emission (gray-level images), dots with slight variation in sizes, and wavelengths encompassing the NIR-I window at 630 nm. The laser system's *x-y* focal point and *z*-axis resolution (full

width at half maximum, FWHM) were set at approximately 0.45 and 0.90 μm, respectively (Fig. 1b). Satisfactory TPA in the NIR-II window was measured using a self-developed femtosecond Ti-sapphire laser optical system, as displayed in Scheme 1; for details of the system, please refer to the Materials section), with an approximately 960 nm extension in subsequent experiments (Fig. 1c). With the application of the most efficient excitation wavelength, the materials can considerably advance relevant two-photon properties applied in bioimaging with TPE [11]. Figure 2a displays the TPL spectra of sorted amino-N-GQDs, with peaks of amino-N-GQD 9.1, amino-N-GQD 9.9, amino-N-GQD 11.1, and amino-N-GQD 12.0 at approximately 719, 772, 810, and 862 nm in the NIR region under TPE (222.7 nJ $pixel^{-1}$ with 20 or 170 scans, approximately 0.13 or 1.11 s of total effective exposure times; Ex: 960 nm). XPS revealed that as the number of carbonyl groups increased (Additional file, Fig. S3), larger electron redistribution appeared, which eventually decreased energy gaps and TPL red shifts [12]. Given that the quadratic dependence of TPL intensifies with the TPE power in the process [13], Fig. 2b confirms the existence of a two-photon process with exponent 2.00 ± 0.02 for sorted dots and conventional fluorophore (e.g., Rhodamine B and Fluorescein; Fig. 2b).

Determination of EWI-TPL phenomenon

The sorted amino-N-GQDs with homogeneous O and N functionalities can be used for investigating intrinsic electronic properties related to optical behavior with quantum confinement, leading to EWI-TPL under TPE. Furthermore, sorted amino-N-GQDs exhibited two-photon stability, which could be attributed to limited photobleaching because of dots' post-TPE TPL intensity (Fig. 2c), whereas that of Rhodamine B and Fluorescein's fluorescence demonstrated poor robustness against photobleaching on TPE exposure (222.7 nJ $pixel^{-1}$ with 20, 100, or 170 scans, approximately 0.13, 0.65, or 1.11 s of total effective exposure times). Furthermore, ultraviolet photoelectron spectroscopy revealed that *n*-state levels were fixed at almost the same energetic positions (6.6–6.8 eV; Additional file, Fig. S6), irrespective of the size determined through TEM and Raman spectroscopy (Additional file, Figs. S2 and S5), which confirmed the highest occupied orbital level of sorted dots. The quantum confinement resulting from the particle size regulated the wavelengths of radiative transitions. Furthermore, EWI-TPL emissions from sorted amino-N-GQDs implied the absence of trap states between the *n*-state and π^* energy levels. A change in the particle size did not cause any disturbance in the *n*-state level. The EWI-TPL of the sorted dots could be attributed to $\pi^* \rightarrow n$ recombination triggering electron transition and phonon scattering. Measurements revealed that the absolute fluorescence QY [14] of the materials ranged from approximately 0.39 (for amino-N-GQD 9.1) to 0.48 (for amino-N-GQD 12.0). Desirable yields were achieved because of the electron-donating species of the sorted amino-N-GQDs structure. XPS revealed that the high percentage of C–N configurations functioned as electron-donation species and improved QY through the inhibition of nonradiative transitions (Additional file, Fig. S3). By contrast, low QY was due to the presence of a large amount of electron-withdrawing carbonyl functional groups acting as nonradiative trap centers (Additional file, Fig. S3). Characterization of sorted amino-N-GQDs revealed successful preparation causes the GQDs to exhibit EWI-TPL characteristics. However, a large cross-section is preferred in the monitoring of molecular actions. Sorted amino-N-GQDs exhibited large absolute TPE cross-section ranging approximately from 55946 to 60728 Goeppert-Mayer (GM; with 1 GM = $10^{-50} cm^4 s$ $photon^{-1}$),

which was more than 2900 times the magnitude of the Fluorescein (~ 19.2 GM; Table 1). The absolute TPE cross section for amino-N-GQD 9.1, amino-N-GQD 9.9, amino-N-GQD11.1, and amino-N-GQD12.0 were approximately 55946, 57332, 59051, and 60728 GM, respectively (Table 2). For detailed calculation, refer to the Materials section. This difference indicates that a high ratio of the energy absorption to the energy input in biospecimens. This phenomenon is highly favorable in two-photon imaging (TPI) [15].

Observation of EM and TPI images during the process of two-photon PDT in the NIR-II window

Because the self-developed optically inverted microscopy system is not suitable for investigating *in vivo* assay processes, the biological environment was mimicked by embedding the *Escherichia coli* (*E. coli*.; 3.98 ± 1.37 μm in length and 0.98 ± 0.34 μm in width calculated from 400 counts of bacteria) strain in a collagen matrix [16]. The TPI action occurred at a specimen depth of 180 μm under TPE (222.7 nJ $pixel^{-1}$ with 20 scans, total effective illumination, ~ 0.13 s; Ex: 960 nm; scan rate, 6.53 ms $scan^{-1}$; scan area, 200×200 μm^2. For details of calculation, refer to the Materials section; Figs. 3a-b). Bacteria was observed clearly under TEM (inset image of Fig. 3a) but was undetectable in the TPL images (Fig. 3a). Lipopolysaccharide (LPS) is the major component of the outer membrane of *E. coli*. The physiologically stable and biocompatible sorted-amino-N-GQDs (Table 4 and Additional file, Fig. S7; the selected concentration of 0.75 μg mL^{-1} material was used in sequential experiments conducted in the dark) were coated with anti-LPS antibody (Ab_{LPS}) through electrostatic interaction to improve efficiency and specificity (Additional file, Scheme S1b), which resulted in the absorption of a substantial amount of sorted dots-Ab_{LPS} on the surface of the bacteria. No exceptional morphology (inset images of Figs. 3b) was observed on the surface of the bacteria. By contrast, when the GQD size was increased from amino-N-GQD 9.1 to amino-N-GQD 12.0, highly fluorescent QY and larger cross-section were detected in the TPL images (Figs. 3b). However, all the photoexcited material–Ab_{LPS}-treated bacteria were severely damaged when the power was increased to 222.7 nJ $pixel^{-1}$ with 100 or 170 scans (with a total effective illumination of ~ 0.65 or ~ 1.11 s), which resulted in abnormal morphology, as observed in TEM (inset images of Figs. 3c and d). TPL decreased after 100 scans (Figs. 3c) and became undetectable after 170 scans (Figs. 3d). For unlabeled bacteria, intrinsic fluorophores' two-photon autofluorescence (TPAF) could not be observed easily under TPE with the same power (Fig. 3e). By contrast, TEM images revealed limited attachment and nonspecific binding for the sorted dot–treated *E. coli* (without coating antibody; 222.7 nJ $pixel^{-1}$ and 20 scans; Ex: 960 nm; inset images of Figs. 3f). Sequentially, TPI also revealed almost no TPL emission at 180 μm (Figs. 3f). Therefore, all the photoexcited sorted dot–treated *E. coli* exhibited no unusual morphology even after photoexcitation (222.7 nJ $pixel^{-1}$ and 170 scans; Ex: 960 nm; inset images of Figs. 3g). Under the same conditions, clear TPI without TPL emission were observed for bacteria without antibody-coated materials (Figs. 3g). However, the images captured at depth > 180 μm contained spherical aberrations, which severely degraded image quality. Such aberrations were caused by the mismatch between the refractive indexes of the aqueous sample and maximal *z* depth of the optical laser system, in addition to the influence of the set objective, detection efficiency, and maximal *z* depth of the optical laser system used [17]. Therefore, TPI was not detected at a 200-μm depth for all the sorted dots (Fig. 4). In this study, the maximum *z* depth for the detection of TPL emissions with the

specific laser optical system was 180 μm because of the detection efficiency and set objective, which was, therefore, set as the optimal depth affording the best resolution for the examination of amino-N-GQDs used as a two-photon contrast probe, particularly for sorted amino-N-GQDs with large lateral size.

Changes in the bacterial cell walls or oxidation were detected. The deterioration of surrounding biological surface substrates was attributable to the reactive oxygen species (ROS), which were through PDT under TPE. These changes may cause bacterial atrophy, morphological damage, and distortion (inset images of Figs. 3c and d) due to amino-N-GQD desorption from the surface of the bacteria (Figs. 3c and d). The LIVE/DEAD kit [18] was used to investigate the green fluorescence of living bacteria (the selected amino-N-GQD 12.0 was used to conduct this experiment; viability > 99%; Additional file, Fig. S8a).The results revealed that the bacteria were almost completely undamaged by exposure to laser treatment (222.7nJ $pixel^{-1}$ with 170 scans; with a total effective illumination of ~ 1.11 s; Ex: 960 nm) with 3h of additional incubation. Photoexcited amino-N-GQD 12.0-Ab_{LPS}-treated bacteria without incubation were also nearly undamaged (viability > 99%; Additional file, Fig. S8b). After 3h of additional incubation, the same panel revealed that dead bacteria were somewhat distinguishable (represented by red fluorescence in Additional file, Fig. S8c). Then, bacterial viability was quantified for further antimicrobial testing, which revealed the almost complete elimination of amino-N-GQD 12.0-Ab_{LPS}-treated bacteria (elimination > 99%; Additional file, Fig. S8d; corresponding to Fig. 3d) and efficient antibacterial effect of amino-N-GQDs in PDT. Thus, no other photochemical activity (e.g., photothermal effect) appeared after photoexcitation. Furthermore, bacteria treated without antibody-coated materials exhibited almost no antimicrobial effect under the same condition (Additional file, Figs. S8e–h; corresponding to Fig. 3g).

ROS assays and bactericidal capability under two-photon PDT

ROS could induce DNA damage, inactivate enzymes, and oxidize amino acid, causing bacterial injury. ROS plays a crucial role in PDT, such as the superoxide radical anion ($O_2^{\cdot -}$) and singlet oxygen ($^1O_2$), which are detectable. Despite the generation of a considerable amount of $^1O_2$ and $O_2^{\cdot -}$, false-positive ROS signals may occur [18] perhaps due to interactions among the sorted amino-N-GQDs, SOSG, *t*-MVP, XTT, and GSH; such signals could affect results (Additional file, Tables S2 and S3). ROS generated by the sorted amino-N-GQD-Ab-treated bacteria was monitored (Additional file, Tables S4 and S5) and appeared to be consistent with the 1270-nm $^1O_2$ phosphorescence signals emitted from the sorted amino-N-GQDs (Fig. 5). The material without antibody coating (Additional file, Tables S6 and S7) generated lower amount of ROS than that produced by the Ab_{LPS}-coated material. Furthermore, $^1O_2$ QY (Φ_Δ) [19] was estimated to be approximately 0.26, 0.28, 0.31, and 0.34 for amino-N-GQD 9.1, amino-N-GQD 9.9, amino-N-GQD 11.1, and amino-N-GQD 12.0, respectively. The study revealed that the material's antimicrobial potential using PDT against *E. coli*. The bactericidal capability of the dots was investigated at a low dose of 0.75 μg mL^{-1} in the dark, with 222.7 nJ $pixel^{-1}$ (20 scans) of TPE (Ex: 960 nm). No significant difference was in the viability of each panel (Additional file, Figs. S9a and b; corresponding to Fig. 3b). With 100 scans, TPE still exhibited no bactericidal effect on bacteria alone and the material in the panel

continued to exhibit considerable biocompatibility with the sorted dots-Ab-treated bacteria without TPE (Additional file, Figs. S9c and d). However, under TPE, sorted amino-N-GQDs displayed excellent bactericidal capability (approximately 89%, 93%, 98%, and 100% elimination for the amino-N-GQD 9.1-Ab_{LPS}, amino-N-GQD 9.9-Ab_{LPS}, amino-N-GQD 11.1-Ab_{LPS}, and amino-N-GQD 12.0-Ab_{LPS}, respectively), amounting to approximately 7.73–7.75 log_{10} reduction (Additional file, Figs. S9c and d; corresponding to Fig. 3c). By contrast, bacterial viability was higher for materials without antibody coating (over 98% viability) than that for materials with the coating (Additional file, Figs. S9c and d). However, although antimicrobial capabilities were still not apparent (approximately 6%,8%, 9%, and 11% elimination for the amino-N-GQD 9.1-, amino-N-GQD 9.9-, amino-N-GQD 11.1-, and amino-N-GQD 12.0-without coating antibody, respectively) sorted dots exhibited 100% antimicrobial efficacy with the number of scans increasing to 170 for all the sorted dots-Ab_{LPS}–treated *E. coli* under TPE (Additional file, Figs. S9e and f; corresponding to Fig. 3d). The results were attributed to sorted amino-N-GQDs functioning as two-photon photosensitizer (PS) to generate ROS that was involved in PDT action. The results also revealed the effectiveness of antibody coating in enhancing the functions of materials.

Effects of nitrogen dopant and amino functionalization

Amino-N-GQDs exhibited remarkable quantum confinement, and their edge effect could be altered to enhance their electrochemical, electrocatalytic, and photochemical activities [4, 6]. The effect of strong electron donation and large π-conjugated system reportedly improves charge transfer efficiency in amino-N-GQDs [20], which resulted in favorable TPA, post-TPE stability, TPE cross-sections, and TPL, as well as a higher ratio radiative and nonradiative decay rates (amino-N-GQD 9.1: 0.64; amino-N-GQD 9.9: 0.69; amino-N-GQD 11.1: 0.82; amino-N-GQD 12.0: 0.92; for calculation, refer the Materials section; Table 2). The results indicate that the material passed mainly through the radiative pathway, as fluorescence QY increased (amino-N-GQD 9.1: 0.39; amino-N-GQD 9.9: 0.41; amino-N-GQD 11.1: 0.45; and amino-N-GQD 12.0: 0.48) and lifetime decreased (from 1.13 to 0.93 ns; Fig. 6, Tables 2 and 3). Radiative electron–hole pair recombination was induced by N dopants and amino groups on the surface of GQD-based material, which boosted intrinsic-state emission. However, as suggested previously, for N dopants and amino groups, the maximum occupied molecular orbital energy of graphene flakes can be increased with the presence of edge amine groups [21]. Thus, the narrowing of orbital band gap boosting PL QY may be caused by resonance between delocalized π orbital and the primary amine's molecular orbital. Furthermore, XPS revealed that C-O, C = O, and amide groups, which induced localized electron–hole pairs' nonradiative recombination and prevented intrinsic-state emission [22], were favorable for small materials (Additional file, Figs. S3 and S4). As the particle size increased, so did PL QY. Moreover, chemical modifications strongly affected the electronic properties of amino-N-GQDs, enabling strong electron donation in primary amine molecules known as amino-group functionalization. Singlet-triplet splitting of amino-N-GQDs results in intersystem crossing and a high triplet state yield. The efficiency of this splitting is sufficient for it to compete with the internal conversion between multiplicity-identical states, which results in the creation of ROS for involvement in PDT [4, 20]. Furthermore, as the number of edge sites increased, the amount of C-N, pyridinic-, amino-, and pyrrolic-N groups increased (Additional file, Figs. S3 and S4). Similarly, as the size of the amino-N-GQDs (Additional file, Figs. S3 and S4)

enlarged (Additional file, Figs. S2 and S5), their antibacterial ability increased and so did the amount of generated ROS (Fig. 5; Additional file, Tables S2-S7), which lead to highly efficient PDT action.

Conclusions

In this study, given the high edge and quantum-confinement effect of GQDs, their intrinsic properties are typically modified through nitrogen functionalization and doping. After TPE, sorted amino-N-GQDs with high crystallinity and uniformity exhibited EWI-TPL in the NIR region as well as favorable electrochemical and photochemical activities. An increase in the mean lateral size, with the increased numbers of the C-N group and enhanced pyridinic-, amino-, and pyrrolic-nitrogen functionalities, induced the radiative recombination of localized electron-hole pairs, leading to favorable TPA and luminescence, absolute cross-section, QY, radiative decay rate, stability and decrease of lifetime. The amounts of ROS generated by and associated with two-photon PDT enhanced the antimicrobial efficacy of a self-developed femtosecond Ti-sapphire laser optical system with low TPE energy and short photoexcitation time (an ultralow energy of 222.7 nJ pixel^{-1} with the short photoexcitation period of 100-170 scans, approximately 0.65-1.11 s of total effective exposure times; excitation wavelength: 960 nm in the NIR-II region). Integration of the materials facilitates a promising two-photon-contrast probe and an efficient two-photon PS in PDT.

Abbreviations

GQD: graphene quantum dot; sorted amino-N-GQDs: sorted nitrogen-doped amino acid–functionalized GQDs; PL: photolumienscence; N-GQDs: GQDs bonded with nitrogen atoms; NIR: near-infrared; EWI-TPL: excitation–wavelength–independent two-photon luminescence; TPE: two-photon excitation; XPS: X-ray photoelectron spectroscopy; TPA: two-photon absorption; QY: quantum yield; PDT: photodynamic therapy; HR-TEM: high-resolution transmission electron microscopy; FWHM: full width at half maximum; TPI: two-photon imaging; *E. coli*.: *Escherichia coli*; LPS: Lipopolysaccharide; Ab_{LPS}: anti-LPS antibody; TPAF: two-photon autofluorescence; ROS: reactive oxygen species; O_2^{-}: superoxide radical anion; $^1O_2$: singlet oxygen; SOSG: Singlet Oxygen Sensor Green; *t*-MVP: trans-1-(2´-methoxyvinyl)pyrene; XTT: 2,3-bis (2-methoxy-4-nitro-5-sulfophenyl)-2H-tetrazolium-5-carboxanilide; GSH: *γ*-L-glutamyl-L-cysteinyl-glycine; PS: photosensitizer.

Declarations

Author's contributions

Wen-Shuo Kuo: Conceptualization, Data Curation, Formal Analysis, Project Administration, Investigation, Methodology, Funding Acquisition, Resources, Software, Supervision, Validation, Visualization. Chia-Yuan Chang and Ping-Ching Wu: Data Curation, Formal Analysis, Investigation, Methodology, Resources, Software, Validation, Visualization. Jiu-Yao Wang: Formal Analysis, Investigation, Methodology,

Resources, Software, Validation, Visualization. The manuscript was written through contributions of all authors. All authors have given approval to the final version of the manuscript.

Author details

[1]Center for Micro/Nano Science and Technology, National Cheng Kung University, Tainan 701, Taiwan (R.O.C.). [2]Allergy & Clinical Immunology Research Center, National Cheng Kung University Hospital, College of Medicine, National Cheng Kung University, Tainan 701, Taiwan (R.O.C.). [3]Advanced Optoelectronic Technology Center, National Cheng Kung University, Tainan 701, Taiwan (R.O.C.). [4]School of Chemistry and Materials Science, Nanjing University of Information Science and Technology, Nanjing 210044, Jiangsu, China. [5]Department of Mechanical Engineering, National Cheng Kung University, Tainan 701, Taiwan (R.O.C.). [6]Department of Biomedical Engineering, National Cheng Kung University, Tainan 701, Taiwan (R.O.C.).

Acknowledgements

Not applicable

Competing interests

This authors that they have no competing interests.

Availability of data and materials

All data generated or analyzed during this study are included in this published article and its Additional files.

Funding

This research was supported by the Ministry of Science and Technology, Taiwan (MOST 108-2314-B-006-053-).

Ethical approval and consent to participate

Not applicable

Consent for publication

Not applicable

References

1. Gong P, Sun L, Wang F, Liu X, Yan Z, Wang M, Zhang L, Tian Z, Liu Z, You J. Highly fluorescent N-doped carbon dots with two-photon emission for ultrasensitive detection of tumor marker and visual

monitor anticancer drug loading and delivery. Chem Eng J. 2019;356:994-1002.

2. Sun Z, Fang S, Hu YH. 3D graphene materials: from understanding to design and synthesis control. Chem Rev. 2020;120:10336-453.
3. Lee J, Wong D, Velasco JrJ, Rodriguez-Nieva, JF, Kahn S, Tsai HZ, Taniguchi T, Watanabe K, Zettl A, Wang F, Levitov LS, Crommie MF. Imaging electrostatically confined Dirac fermions in graphene quantum dots. Nat Phys. 2016;12:1032-6.
4. Wang X, Li X, Zhang L, Yoon Y, Weber PK, Wang H, Guo J, Dai H. N-doping graphene electrothermal reactions with ammonia. Science. 2009;324:768-71.
5. Zhao G, Li X, Huang M, Zhen Z, Zhong Y, Chen Q, Zhao X, He Y, Hu R, Yang T, Zhang R, Li C, Kong J, Xu LB, Ruoff RS, Zhu H. The physics and chemistry of graphene-on-surfaces. Chem Soc Rev. 2017;46:4417-49.
6. Torres, T. Graphene chemistry. Chem Soc Rev. 2017;46:4385-6.
7. Yildirim M, Sugihara H, So PTC, Sur M. Functional imaging of visual cortical layers and subplate in awake mice with optimized three-photon microscopy. Nat Commun. 2019;10; https://doi.org/10.1038/s41467-018-08179-6
8. Kim L, Kim S, Jha PK, Brar VW, Atwater HA. Mid-infrared radiative emission from bright not plasmons in graphene. Nat Mater. 2021; https://doi.org/10.1038/s41563-021-00935-2
9. Liu Q, Guo B, Rao Z, Zhang B, Gong JR. Two-photon-induced fluorescence from photostable, biocompatible nitrogen-doped graphene quantum dots for cellular and deep-tissue imaging. Nano Lett. 2013;13:2436–41.
10. Hummers WS, Offeman RE. Preparation of graphitic oxide. J Am Chem Soc. 1958;80:1339.
11. Zhao W, Li Y, Yang S, Chen Y, Zheng J, Liu C, Qing Z, Li J, Yang R. Two-photon excitation/red emission, ratiometric fluorescent nanoprobe for intracellular pH imaging. Anal Chem. 2016;88:4833-40.
12. Liu J, Li D, Zhang K, Yang M, Sun H, Yang B. One-step hydrothermal synthesis of nitrogen-doped conjugated carbonized polymer dots with 31% efficient red emission for *in vivo* imaging. Small. 2018;14; https://doi.org/10.1002/smll.201703919
13. Horton NG, Wang K, Kobat D, Clark CG, Wise FW, Schaffer CB, Xu C. *In vivo* three-photon microscopy of subcortical structures within an intact mouse brain. Nat Photonics. 2013;7:205-9.
14. Würth C, Grabolle M, Pauli J, Spieles M, Resch-Genger U. Relative and absolute determination of fluorescence quantum yields of transparent samples. Nat Protoc. 2013;8:1535-50.
15. Li B, Wu C, Wang M, Charan K, Xu C. An adaptive excitation source for high-speed multiphoton microscopy. Nat Methods. 2020;17:163-6.
16. Roy B, Yuan L, Lee Y, Bharti A, Mitra A, Shivashankar GV. Fibroblast rejuvenation by mechanical reprogramming and redifferentiation. Proc Natl Acad Sci USA. 2020;117:10131-41.
17. Richardson DS, Lichtman JW. Clarifying tissue clearing. Cell. 2015;162:246-57.

18. Kuo WS, Chen HH, Chen SY, Chang CY, Chen PC, Hou YI, Shao YT, Kao HF, Hsu CLL, Chen YC, Chen SJ, Wu SR, Wang JW. Graphene quantum dots with nitrogen-doped content dependence for highly efficient dual-modality photodynamic antimicrobial therapy and bioimaging. Biomaterials. 2017;120:185-94.'
19. Shi L, Hernandez B, Selke M. Singlet oxygen generation from water-soluble quantum dot-organic dye nanocomposites. J Am Chem Soc. 2006;128:6278-9.
20. Son DT, Kwon BK, Park DH, Seo WS, Yi Y, Angadi B, Lee CL, Choi WK. Emissive ZnO-graphene quantum dots for white-light-emitting diodes. Nat Nanotechnol. 2012;7:465-71.
21. Tetsuka H, Asahi R, Nagoya A, Okamoto K, Tajima I, Ohta R, Okamoto A. Optically tunable amino-functionalized graphene quantum dots. Adv Mater. 2012;24:5333-8.
22. Bao L, Zhang ZL, Tian ZQ, Zhang L, Liu C, Lin Y, Qi B, Pang DW. Electrochemical tuning of luminescent carbon nanodots: from preparation to luminescence mechanism. Adv Mater. 2011;23:5801-6.

Tables

Table 1 TPE cross section of materials at excitation wavelength of 960 nm. Delivered dose: 0.75 μg mL^{-1} material.

Reference	Integrated emission intensity (counts)		Action cross-section (ησ)
Rhodamine B[a]	53.9		13.4
Analyte	**Integrated emission intensity (counts)**	**Absolute quantum yield (η)**	**Absolute cross-section (σ)**
amino-N-GQD 9.1	87754	0.39	55946
amino-N-GQD 9.9	94550	0.41	57332
amino-N-GQD 11.1	106887	0.45	59051
amino-N-GQD 12.0	117250	0.48	60728
Fluorescein	61.1	0.79[b]	19.2

[a]Rhodamine B was selected as a reference to determine the TPE cross section. The relevant calculations are shown in the Materials section. [b]Forster LS, Livingston R. The absolute quantum yields of the fluorescence of chlorophyll solutions. J Chem Phys. 1952;20:1315–20.

Table 2 Two-photon properties of the sorted amino-N-GQDs. Delivered dose: 0.75 μg mL^{-1} material.

	Absolute cross QY (GM)	Absolute section of TPE	Lifetime Radiative (ns)	Decay rate (x 10^8 s^{-1})	Nonradiative Decay rate (x 10^8 s^{-1})	Ratio of radiative to nonradiative decay rates
amino-N-GQD 9.1	0.39	55946	1.13	3.45	5.40	0.64
amino-N-GQD 9.9	0.41	57332	1.09	5.41	5.30	0.69
amino-N-GQD 11.1	0.45	59051	1.04	4.33	5.29	0.82
amino-N-GQD 12.0	0.48	60728	0.93	5.16	5.59	0.92

Table 3 The lifetime data and the parameter generated using a time-correlated single-photon counting technique involving a triple-exponential fitting function while monitoring the emission under TPE. Delivered dose: 0.75 µg mL^{-1} material.

	Absolute cross QY (GM)	Absolute section of TPE	Lifetime Radiative (ns)	Decay rate (x 10^8 s^{-1})	Nonradiative Decay rate (x 10^8 s^{-1})	Ratio of radiative to nonradiative decay rates
amino-N-GQD 9.1	0.39	55946	1.13	3.45	5.40	0.64
amino-N-GQD 9.9	0.41	57332	1.09	5.41	5.30	0.69
amino-N-GQD 11.1	0.45	59051	1.04	4.33	5.29	0.82
amino-N-GQD 12.0	0.48	60728	0.93	5.16	5.59	0.92

Table 4 Stability of the newly prepared and as-prepared sorted-amino-N-GQD for 3 months in physiological environment of the culture medium for *E. coli* determined by Raman (Additional file, Equations S9-S10) and zeta potential spectroscopy. [Cell type for zeta potential: DTS1060C; Measurement duration: 30 number of runs, 20 run duration (sec)]. Delivered dose: 7.5 mg mL^{-1} material.

Mean lateral size (nm)/ Zeta potential (mV)	Newly prepared	As-prepare for 3 months
amino-N-GQD 9.1-Ab_{LPS}	9.0 nm/ 6.2 mV	9.1 nm/ 6.4 mV
amino-N-GQD 9.9-Ab_{LPS}	9.9 nm/ 7.9 mV	10.0 nm/ 8.0 mV
amino-N-GQD 11.1-Ab_{LPS}	11.2 nm/ 9.0 mV	11.2 nm/ 9.1 mV
Amino-N-GQD 12.0-Ab_{LPS}	11.9 nm/ 9.6 mV	12.0 nm/ 9.8 mV

Figures

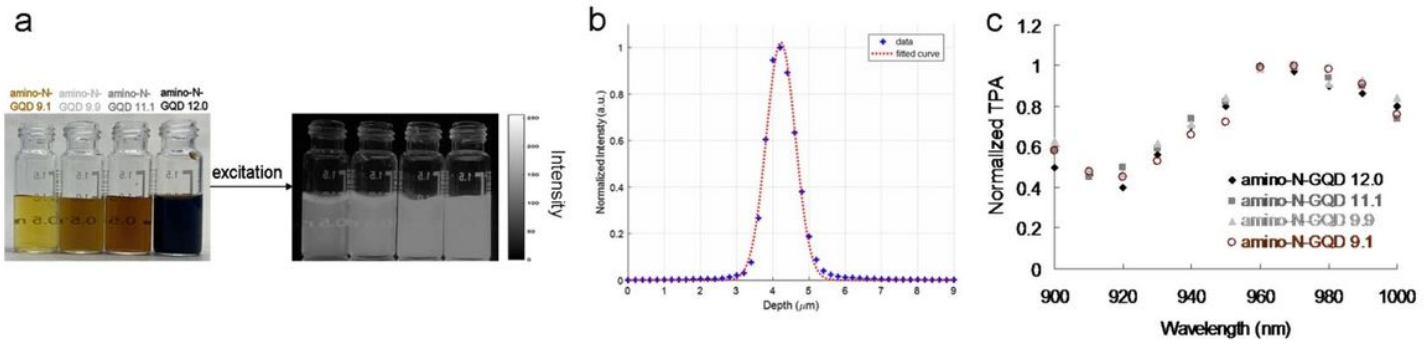

Figure 1

a Photographs of materials without and with 630 nm (gray level) light excitation. b Z-axis scan of a thin gold film for measuring the second harmonic generation signal at various positions. The laser system's z-axis resolution (FWHM) was 0.90 μm (fit using the Gaussian function). c Relative TPA spectra of the sorted amino-N-GQDs. TPE signals were obtained at wavelengths 900–1000 nm and at 127.3 nJ pixel−1. Delivered dose: 0.75 μg mL−1 material.

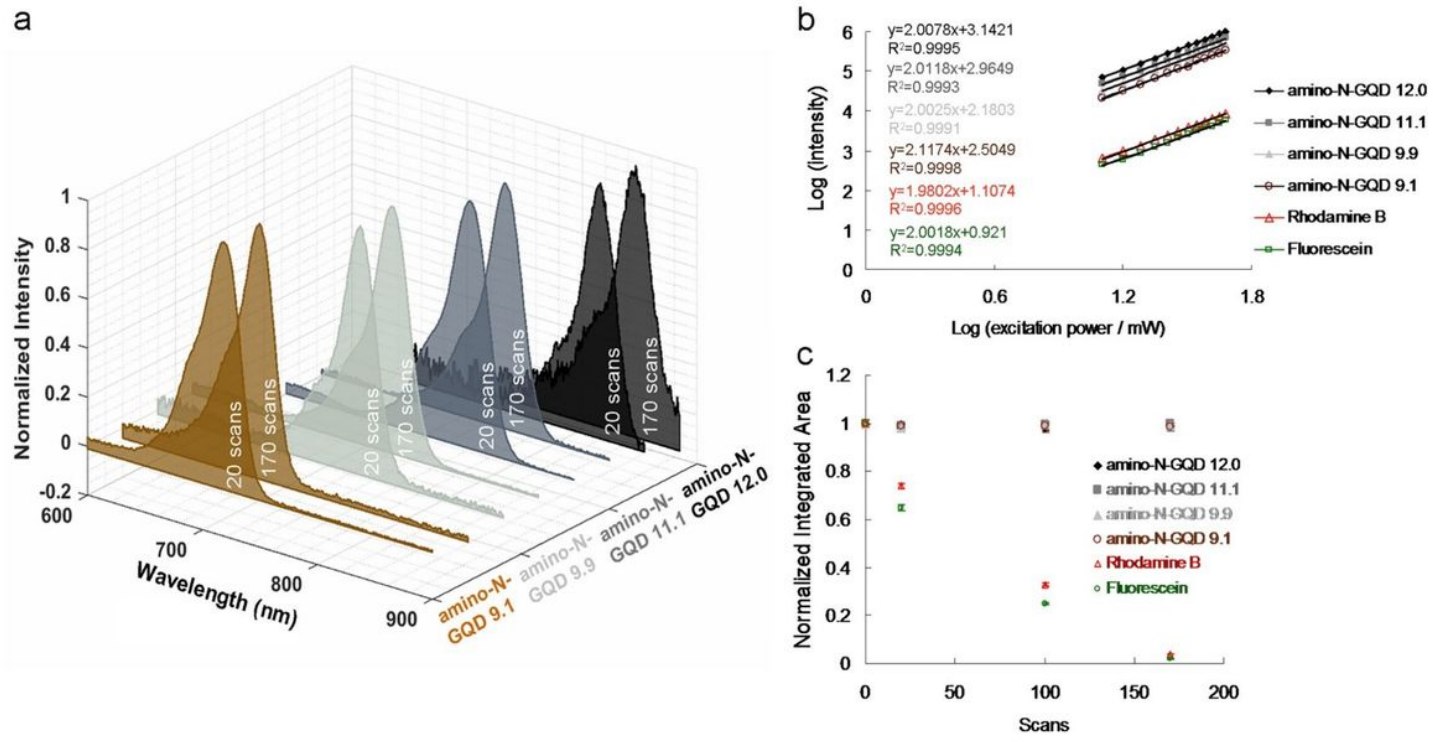

Figure 2

a Relative TPL spectra of materials for TPE power= 222.7 nJ pixel−1 [20 and 170 scans (total effective exposure times, ~0.13 s and ~1.11 s), respectively; cut off= 900 nm, as determined using cascading filters]. b TPL intensity dependence on the excitation power (logarithm) of materials and fluorophores; the slope is approximately 2.00 ± 0.02. TPE power= 1272.8-5091.2 nJ pixel−1; R2> 0.999. c Two-photon stability of amino-N-GQDs, Rhodamine B and Fluorescein under TPE of power= 222.7 nJ pixel−1 with 20, 100, and 170 scans. The normalized integrated area was calculated by dividing emission intensities of the integrated area after photoexcitation by those of the newly prepared material without photoexcitation. Delivered dose: 0.75 µg mL−1 material. Data are presented in the mean ± standard deviation form (n=6).

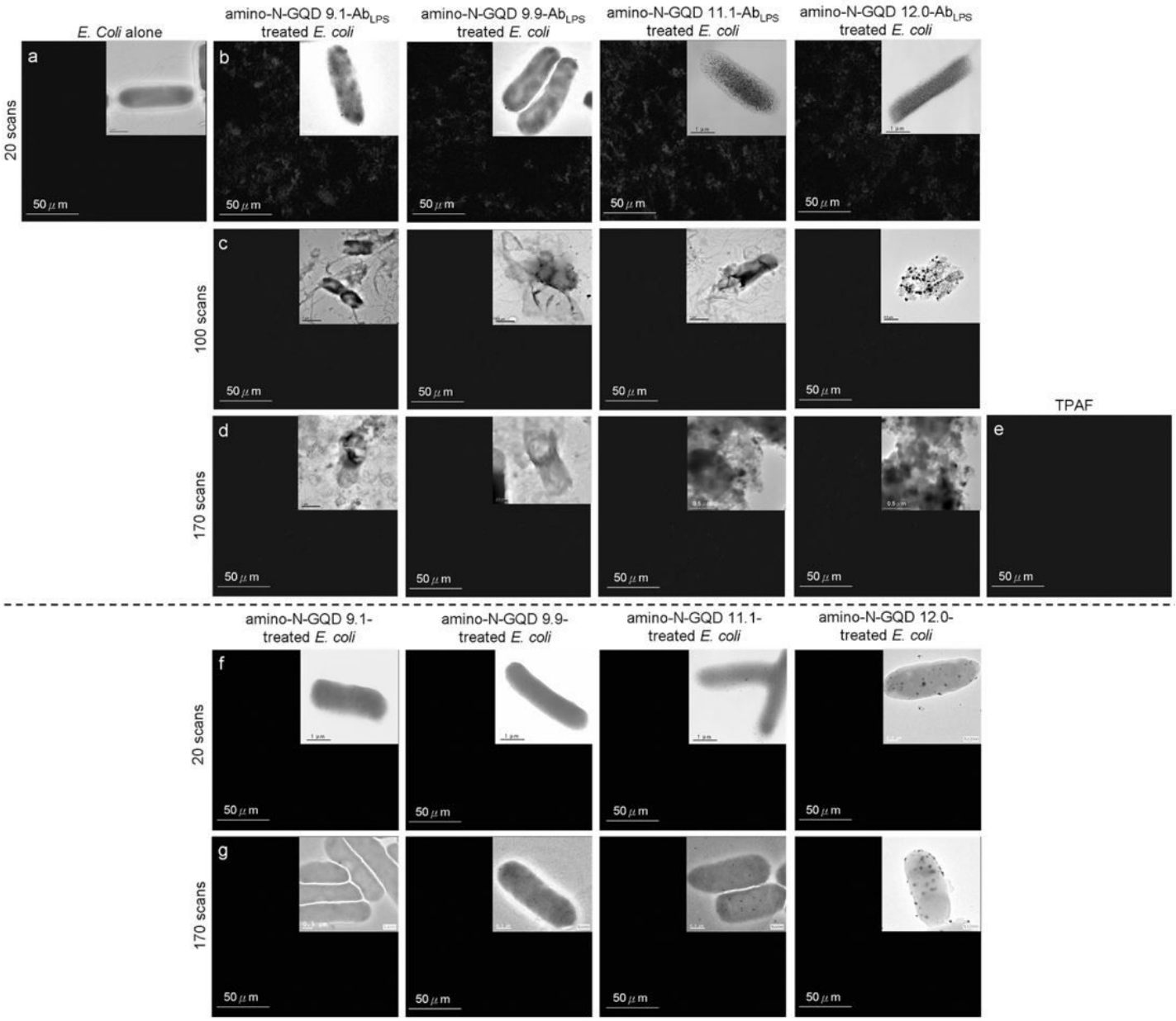

Figure 3

TPL images (gray level) of a E. coli and bacteria subjected to sorted amino-N-GQD-AbLPS treatment, observed at a 180-μm depth (222.7 nJ pixel−1) with b 20 scans and c 100 scans through TPE. d Images acquired after an additional 170 scans were performed. e TPAF image of the unlabeled bacteria. TPL images of bacteria treated without antibody-coated materials with f 20 scans and g 170 scans through photoexcitation under the same condition. TEM images illustrating a, inset bare E. coli, b-d, insets sorted amino-N-GQD-AbLPS-treated E. coli and f-g, insets sorted amino-N-GQD-treated E. coli with the same treatments as in a-d and f-g. All images were acquired after 3 h of additional incubation. TPE wavelength: 960 nm. Delivered dose: OD600:~0.05 of E. coli or 0.75 μg mL−1 material-AbLPS.

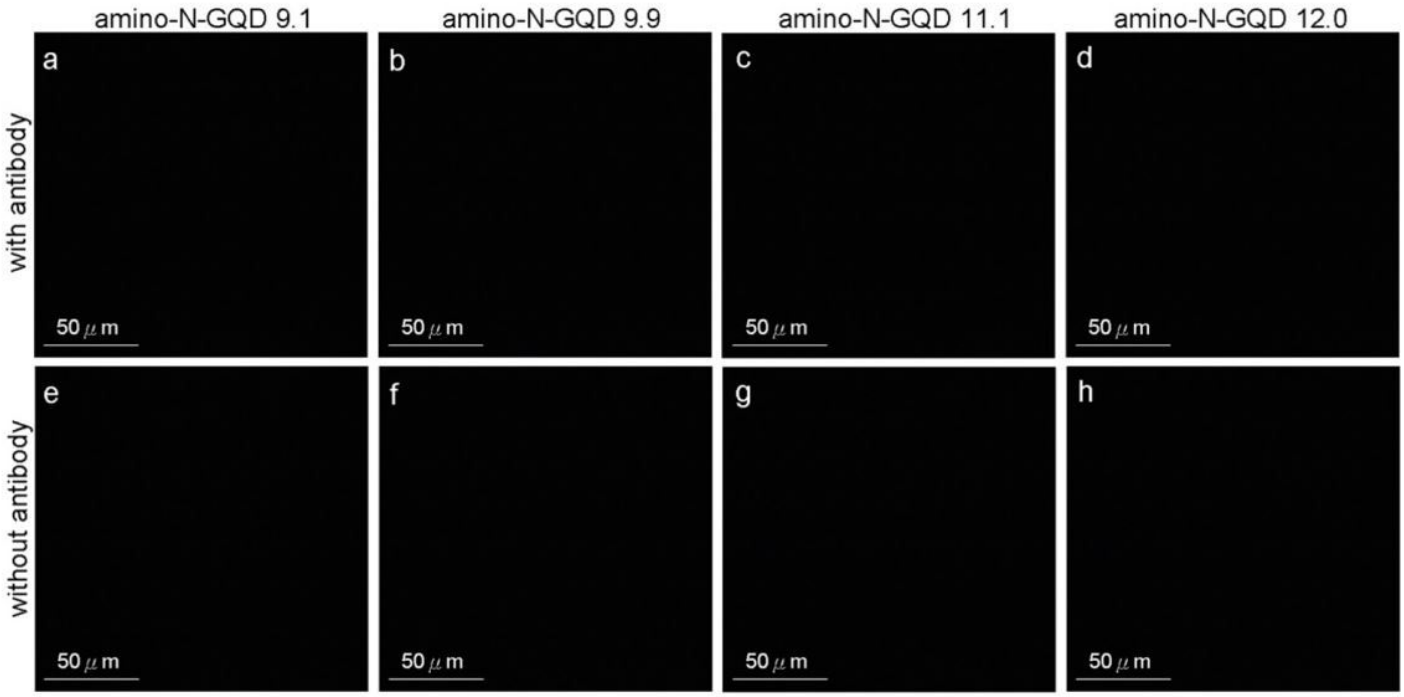

Figure 4

TPL images (gray level) of E. coli subjected to the a,e amino-N-GQD 9.1, b,f amino-N-GQD 9.9, c,g amino-N-GQD 11.1, and d,h amino-N-GQD 12.0 a-d with or e-h without antibody coating treatments and incubated for 3 h, observed at a 200-μm depth (222.7 nJ pixel−1 with 170 scans, approximately 1.11 s of total exposure time) by TPE (Ex: 960 nm). Delivered dose: OD600:~0.05 of E. coli; 0.75 μg mL−1 material or 0.75 μg mL−1 material-AbLPS.

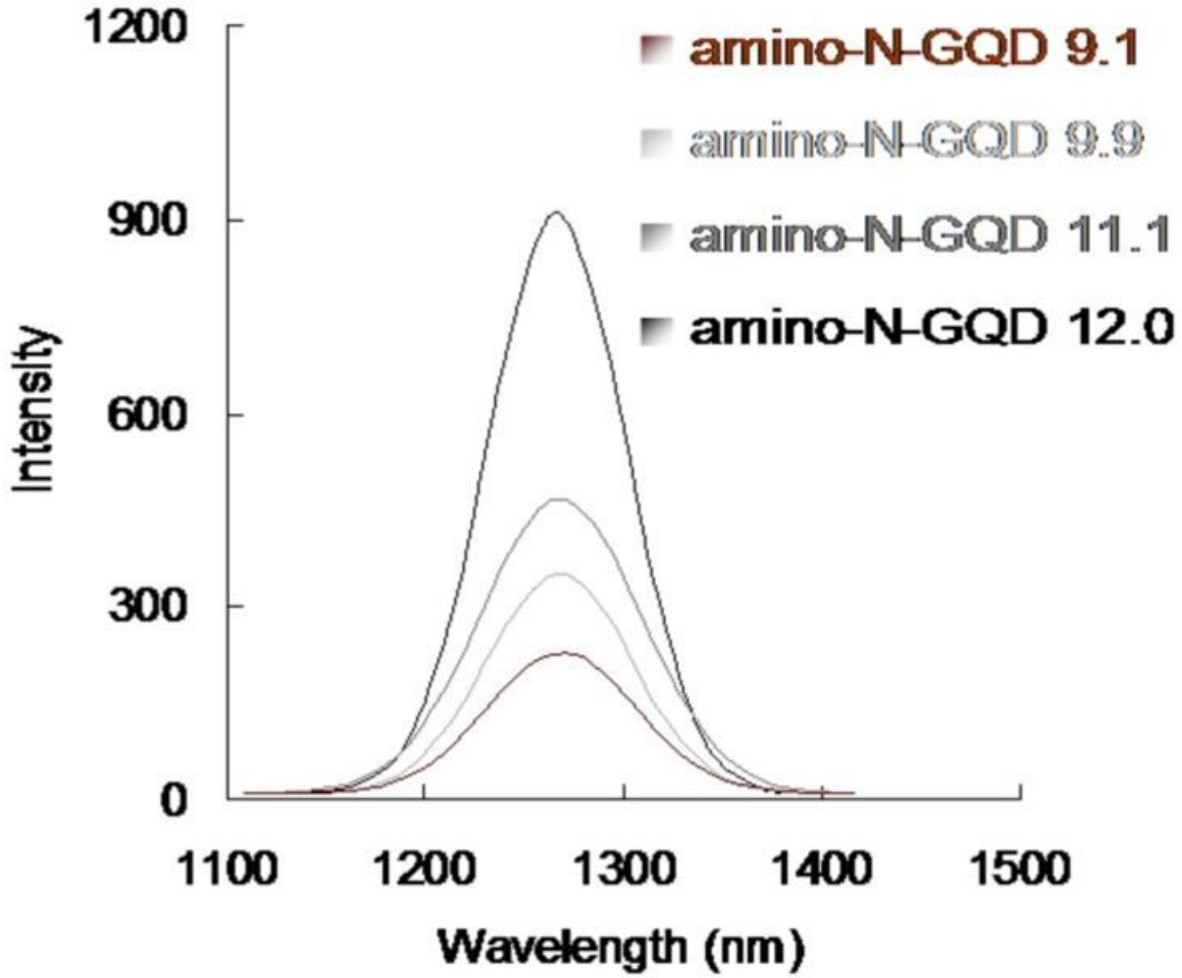

Figure 5

Phosphorescence spectra of the sorted amino-N-GQDs (obtained at 1270 nm). Delivered dose: 0.75 μg mL−1 material.

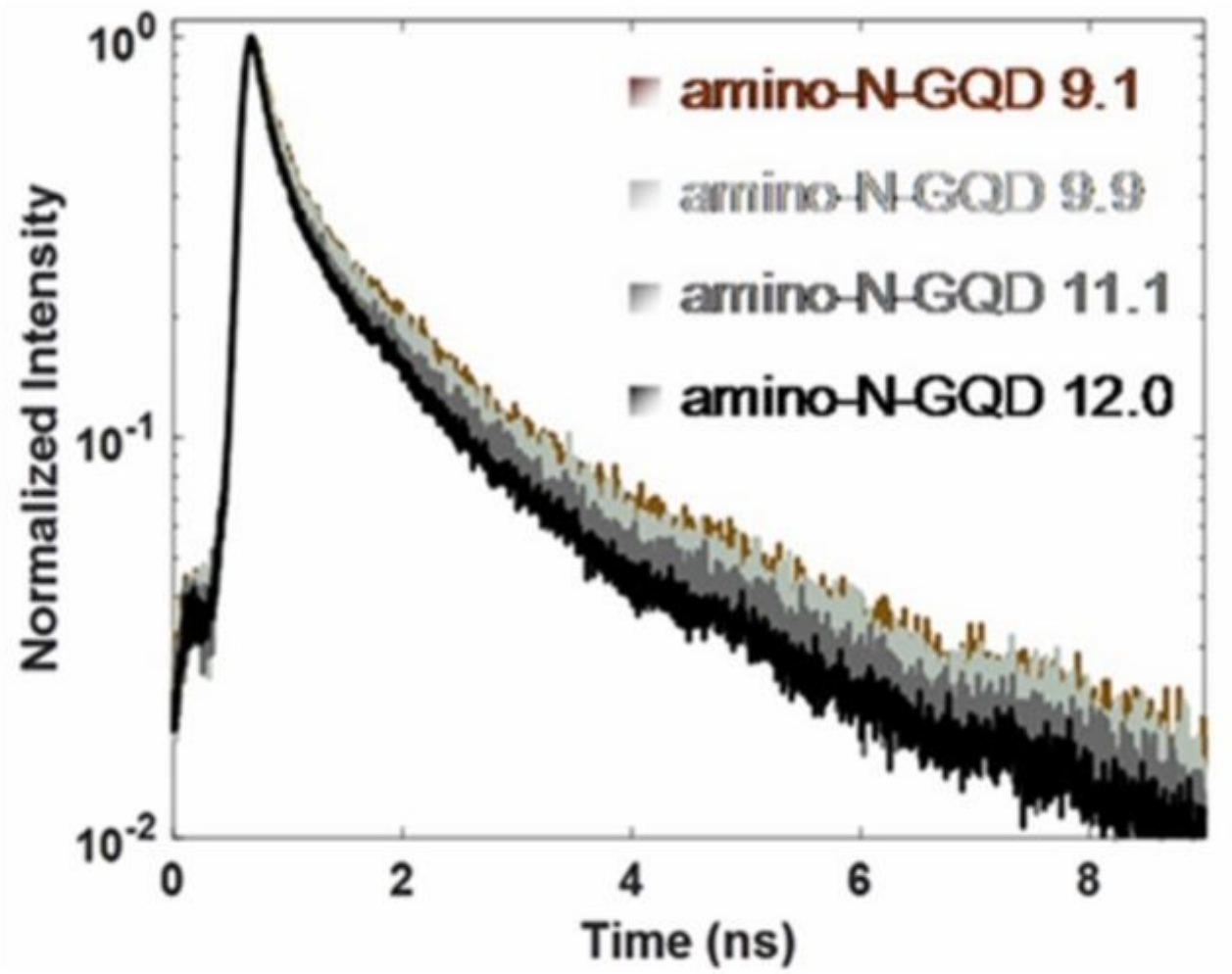

Figure 6

Time-resolved room-temperature TPL material decay profiles at room temperature. Delivered dose: 0.75 µg mL−1 material.

Supplementary Files

This is a list of supplementary files associated with this preprint. Click to download.

- scheme1.jpg
- Additionalfile.pdf